

NJC

Accepted Manuscript



This is an *Accepted Manuscript*, which has been through the Royal Society of Chemistry peer review process and has been accepted for publication.

Accepted Manuscripts are published online shortly after acceptance, before technical editing, formatting and proof reading. Using this free service, authors can make their results available to the community, in citable form, before we publish the edited article. We will replace this *Accepted Manuscript* with the edited and formatted *Advance Article* as soon as it is available.

You can find more information about *Accepted Manuscripts* in the [Information for Authors](#).

Please note that technical editing may introduce minor changes to the text and/or graphics, which may alter content. The journal's standard [Terms & Conditions](#) and the [Ethical guidelines](#) still apply. In no event shall the Royal Society of Chemistry be held responsible for any errors or omissions in this *Accepted Manuscript* or any consequences arising from the use of any information it contains.

Cite this: DOI: 10.1039/c0xx00000x

www.rsc.org/xxxxxx

ARTICLE TYPE

Synthesis and magnetic properties of samarium hydroxide nanocrystals

Xusheng Zheng,^a Li Song,^a Shoujie Liu,^a Tiandou Hu,^b Jiafu Chen,^c Xing Chen,^a Augusto Marcelli,^{a,d} Muhammad Farooq Saleem,^a Wangsheng Chu,^{*a,b} and Ziyu Wu^{*a,b}

Samarium hydroxide (Sm(OH)₃) is an important samarium compound with many potential applications in electronics, optics and catalysis. Based on a facile hydrothermal method assisted by oleic acid surface modifications we synthesized Sm(OH)₃ nanocrystals with various morphologies. In this system, by adding oleic acid surfactant both crystallization and grain size of nanocrystals can be tuned. Furthermore, the paramagnetic resonance and magnetic measurements point out that rod-like Sm(OH)₃ are non-magnetic, while Sm(OH)₃ disc-like samples exhibit a weak ferromagnetism. The correlation between magnetism and morphology in Sm(OH)₃ nanocrystals is associated to the surfactant-induced surface modification as well as to the changes of electron's localization in Sm 5d orbitals, in agreement with X-ray absorption spectroscopy data.

1 Introduction

Because of their unique properties, nanosized rare-earth (RE) materials with different size and shape triggered a large interest in the recent years. Many successful technological researches have been published,^{1,2,3} and others have been proposed using luminescent materials,^{4,5} catalysts^{6,7}, etc. The chemistry of layered RE hydroxides with anion-exchange properties^{8,9,10,11} explains their properties and allows tuning electronic, magnetic and optical properties of similar systems.¹² Efforts have been made to study pure RE hydroxides and oxide nanocrystals. As an example, Xu *et al.*¹³ described the synthesis and characterization of Ln(OH)₃ and Ln₂O₃ sub-microspindles. Ghosh *et al.*¹⁴ reported the synthesis of Sm₂O₃ nanocrystals with different shapes, while the microarchitectures of lanthanide oxide have been synthesized via an ethylene glycol mediated hydrothermal method and their luminescent properties investigated by Jun Yang *et al.*¹⁵ Among the most important RE based materials, samarium compounds offer numerous applications in biomedicine,¹⁶ nanoelectronics,¹⁷ solar cells,^{12, 18} catalysis¹⁹ and again luminescent materials.²⁰ The microstructures of samarium compounds, including grain size, shape and crystallinity, play a key role to control properties. Different methods have been used to tune size and shape of RE oxide or hydroxide nanocrystals: sol-gel processes,²¹ irradiation treatments,²² reverse micelles,^{14,23} hydrothermal methods,²⁴ etc. Among them, hydrothermal methods, which are based on the phase transfer and reaction at the interface between a solvent and water phases, offers many advantages: high crystallinity, excellent stability and an easy tunability.^{25,26} In these methods surfactants play a key role in controlling both the growth and stability of nanocrystals.^{27,28} A variety of nanomaterials such as CeO₂^{29,30} or Sm₂O₃³¹ have been prepared with this method using different surfactants.

Recently, studies reported the observation of ferromagnetism in pure lanthanide oxides and hydroxides nanoparticles such as CeO₂, which are not observed in the corresponding bulk systems. The phenomenon points out the role of oxygen vacancies in these

room temperature ferromagnetic systems^{32,33}.

In this research, we used a facile surfactant-assisted hydrothermal method to successfully synthesize samarium hydroxide nanocrystals with different morphologies. The concentration of oleic acid (OA) surfactant plays a key role to control the shape of Sm(OH)₃ nanocrystals. Moreover, in contrast with the non-magnetic behaviour of rod-like Sm(OH)₃ samples, disc-like Sm(OH)₃ nanocrystals exhibit a weak ferromagnetism that we associate to surfactant-induced surface modifications and to the localization of electronic states in Sm 5d orbitals.

2 Experimental

2.1 Sample synthesis

Samarium hydroxide nanocrystals were synthesized by a facile surfactant-assisted hydrothermal method. The samarium nitrate hexahydrate (99.9%) and OA (90%) were purchased from Alfa Aesar Company. The sodium hydroxide and the analytical grade ethanol were purchased from Shanghai Chemical Company. All chemicals were used as received without further purification. For synthesis, 30 ml of 25 mmol/L samarium nitrate aqueous solutions were mixed with 0, 0.1, 0.3 and 1 ml of OA. Then, 4 mol/L sodium hydroxide solution was slowly dropped into the above indicated mixture solution with a magnetic stirring. The pH value was maintained at 10 during the process. The reaction mixtures were stirred for ~30 min to obtain white precipitates. The resulting micro-emulsions were transferred to a 50 ml Teflon-lined stainless-steel autoclave, then sealed and maintained at 180 °C for 24 h. The obtained suspensions were cooled to room temperature, naturally. The precipitates were then collected by centrifugation (9000 rpm) and washed with distilled water and ethanol for three times. Finally, a series of nanocrystals was obtained after drying at 50 °C for 12 h.

2.2 Characterization

The composition and the phase of the as-prepared products were determined by X-ray diffraction (XRD), using a Philip X'Pert PROSUPER γA rotation anode with Cu Kα radiation (λ =

1.54187 Å) at 25 °C. Transmission electron microscopy (TEM) images were collected with a JEOL-2010 transmission electron microscope operating at 120 kV. Electron paramagnetic resonance (EPR) experiments were performed with a JES-FA200 JEOL spectrometer at room temperature, microwave frequency 9.06 GHz, power 1 mW, field modulation width 0.35 mT, sweep time 1 min and time constant 0.3 s. X-ray absorption spectroscopy (XAS) at the Sm L₃ edge was performed in the transmission mode using a double crystal Si (111) monochromator at the beamline 1W2B of the Beijing Synchrotron Radiation Facility (BSRF). The storage ring energy was 2.5 GeV with an average electron current of 150 mA. The incident and output beam intensities were monitored by ionization chambers filled with pure nitrogen. To suppress the higher harmonics content in the low energy range, crystals were detuned with a reduction of ~30% of the incident beam intensity. Magnetic measurements were carried out using a superconducting quantum interference device (SQUID) under a magnetic field of 5 kOe in the range 5 - 300 K.

3 Results and discussion

3.1 Morphology and crystallography evolutions

The morphology and microstructure details of synthesized products were investigated by TEM and high-resolution transmission electron microscopy (HRTEM). Fig. 1(a) shows a TEM image of a rod-like Sm(OH)₃ synthesized with no OA. The average length of these nanorods is ~160 nm with an average width of ~20 nm. After addition of 0.1 ml OA, the length of Sm(OH)₃ nanorods reduces to 80 ~ 100 nm and as shown in fig. 1(b), few samples with sheet-like morphology appears. In our experiments concurrent broadening in the shape of nanosheets is observed with the increase in concentration of OA. Fig. 1(c) shows the morphology of Sm(OH)₃ nanosheets with an average length of 200 nm synthesized with 0.3 ml OA. However, a more interesting phenomenon occurs when the concentration of OA increases up to 1 ml. Above this value, the morphology of Sm(OH)₃ nanosheets abruptly changes to a disc-like shape with a diameter of ~200 nm (Fig. 1(d)).

To further characterize the microstructure of Sm(OH)₃ samples, we collected HRTEM images and the corresponding selected area electron diffraction (SAED) patterns, as shown in Fig. 1(a1-d1). Fig. 1(a1) points out that as-prepared nanorods are characterized by a high crystallinity, actually comparable to single crystal samples. The image also displays a cross-lattice pattern with an interplanar spacing of 0.30 nm. The image and data suggest that the exposed faces of nanocrystals are (101), in good agreement with the JCPDS 06-0117 standard. After addition of more OA, multi-crystal domains appear and polycrystalline Sm(OH)₃ nanocrystals are also formed, as shown in Fig. 1(b1-d1). In other words, increasing the amount of the surfactant OA, the as-prepared Sm(OH)₃ nanocrystal samples can be obtained as single-crystals or as polycrystalline samples. In particular, SAED of Sm(OH)₃ nanorods shows ordered diffraction patterns, while Sm(OH)₃ nanodiscs exhibit typical polycrystalline diffraction rings, in agreement with XRD patterns discussed below.

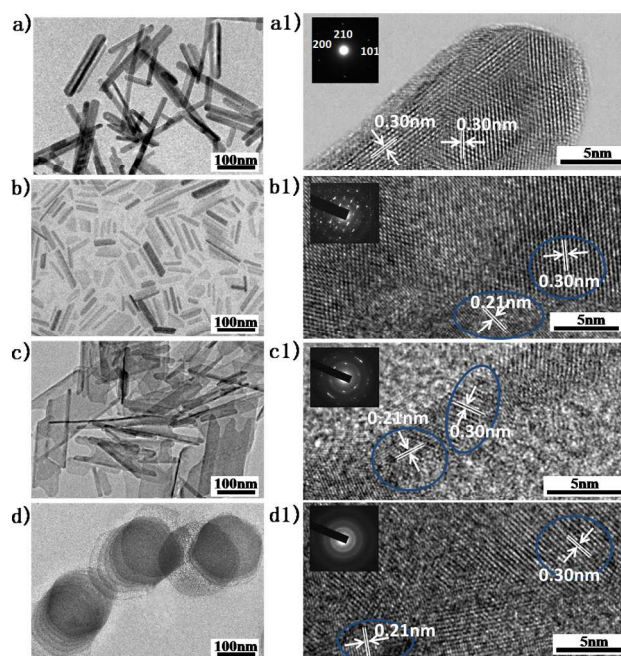


Fig. 1 TEM and HRTEM images of Sm(OH)₃ nanocrystals synthesized by the hydrothermal method for different amounts of OA: (a, a1) 0 ml, (b, b1) 0.1 ml, (c, c1) 0.3 ml, (d, d1) 1 ml. The insets show selected area electron diffraction (SAED) patterns of each sample.

XRD patterns have been collected to identify the crystalline structure of the as-synthesized Sm(OH)₃ samples and the XRD pattern of the sample without OA is shown in Fig. 2(a). The standard samarium hydroxide database (Joint Committee for Power Diffraction Studies (JCPDS) file No.06-0117) is also shown in Fig. 2 to identify materials.

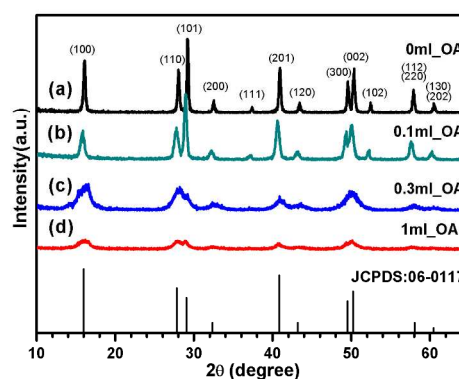


Fig. 2 XRD patterns of the Sm(OH)₃ nanocrystals shown in Fig. 1.

The intense peaks observed have been indexed as hexagonal phase associated to a crystalline form of a pure Sm(OH)₃. The patterns (b,c) in Fig. 2 are XRD data of samples synthesized with 0.1 ml and 0.3 ml of OA. Their peaks are broader and weaker. Increasing the amount of OA the changes are even more evident. Crystallinity and dimension of nanocrystals can be reduced

increasing the OA. Indeed, when the oleic acid proportion reaches 1ml, the detected changes (see panel d) point out a simultaneous decrease in the crystallinity and of the particle size. In other words, both crystallinity and lattice sizes of $\text{Sm}(\text{OH})_3$ nanocrystals are affected by the amount of the surfactant.

3.2 Magnetic properties

To characterize magnetic properties of $\text{Sm}(\text{OH})_3$ nanocrystals, we collected EPR spectra (fig. 3). From EPR data we may clearly see that in these $\text{Sm}(\text{OH})_3$ nanocrystals the g value increases going from nanorods ($g \sim 2.0$) to nanodiscs ($g > 2.3$). These results suggest the presence of a weak ferromagnetic character only in $\text{Sm}(\text{OH})_3$ nanodiscs. As a rare earth element, the electronic configuration of Sm^{3+} is $4f^5$ with a free-ion ground state $^6\text{H}_{5/2}$.³⁴ Interaction with the crystalline electric field is much weaker than the spin-orbit coupling.³⁵ Thus the $\text{Sm}(\text{OH})_3$ usually exhibits a paramagnetic behaviour with a g -value similar to a free electron, which is 2.0.³⁶ When g increases, the orbital moment increases and the magnetic properties of the material improve.³⁷ The higher g -value (in panel d: $g > 2.3$) implies that $\text{Sm}(\text{OH})_3$ nanodiscs may have weak ferromagnetic properties.

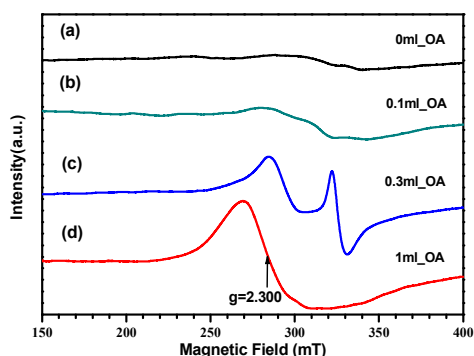


Fig. 3 EPR spectra of differently shaped $\text{Sm}(\text{OH})_3$ nanocrystals: (a) nanorods (no surfactant assisted), (b) wide nanorods (0.1 ml OA assisted), (c) nanosheets (0.3 ml OA assisted), (d) nanodiscs (1 ml OA assisted).

We also measured the field dependent magnetization of $\text{Sm}(\text{OH})_3$ samples. In fig. 4 we compare the magnetic-field dependence of the magnetization (M - H) at 5 and 300 K of $\text{Sm}(\text{OH})_3$ nanodiscs (the field dependent magnetization behavior of nanorods and nanosheets is included in the supplementary information). The magnetization curve shows that nanodiscs are mainly paramagnetic with only a weak ferromagnetic character. After the subtraction of the paramagnetic contribution and a linear fit, we estimated that the saturation moment of the sample at 300 K and 5 K is 0.14 and 0.12 emu/g, respectively. In order to characterize $\text{Sm}(\text{OH})_3$ nanodisc samples at the atomic/electronic level, we also performed Sm L_3 -edge XANES experiments.

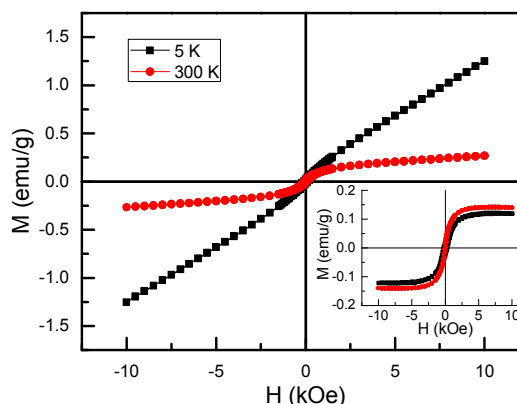


Fig. 4 Field dependent magnetization of $\text{Sm}(\text{OH})_3$ nanodiscs. In the inset the hysteresis loop after subtraction of the paramagnetic contribution.

3.3 Correlation between magnetism and morphology

Fig. 5 shows normalized Sm L_3 -edge XANES spectra of the as-prepared samples. All spectra have similar features, indicating that the chemical configuration around Sm atoms is the same in different $\text{Sm}(\text{OH})_3$ samples. Moreover, the white lines of the spectra are characterized by only a strong single-peak at ~ 6723 eV, rather than a double-peak feature characteristic of mixed valence state materials such as CeO_2 ³⁸ or other mixed-valence RE-containing compounds.^{39, 40} The single-peak feature is typical of a trivalent RE system whose oxidation state is shared in all as-prepared samples. In other words, the valence state of $\text{Sm}(\text{OH})_3$ nanocrystals is not affected by surface processes. The stability of the Sm valence also rules out any possible contribution from local chemical configurations that affects magnetic properties in many oxides and metal compounds.⁴¹ However, the intensity of the white line differs in these $\text{Sm}(\text{OH})_3$ samples, i.e., the white line intensity decreases when the surfactant concentration increases. In the framework of the multiple scattering (MS) theory, the white line is associated to multiple scattering processes within the first shell (i.e., the hydroxyl groups) around the photoabsorber.^{42, 43} However, the decrease of the intensity of the white line points out also a decrease of the local partial empty density of states around the Sm site, a phenomenon that can be correlated to the removal of the hydroxyl groups around Sm due to the surfactant OA. These surface modifications generated oxygen vacancies around the Sm atom.

XRD and TEM results above discussed point out that the surface-to-volume ratio increases with the amount of the surfactant. The behavior is in agreement with an increasing number of hydroxyl vacancies generated at the surface of the modified $\text{Sm}(\text{OH})_3$ samples. Pioneering works on CeO_2 ^{31, 44} show that oxygen vacancies may induce a magnetic moment on neighboring Ce ions. This mechanism can explain why a ferromagnetic behavior appears only when the concentration of the OA reaches 1 ml and the origin of this weak ferromagnetism. Actually, only surface Sm atoms, which bound up hydroxyl vacancies, contribute to the magnetic moment. When the concentration of vacancies becomes large, then a ferromagnetic character is observed.

We can also discuss the mechanism generating the ferromagnetism in the $\text{Sm}(\text{OH})_3$ starting from the electronic structure. Indeed, the Sm L-edge corresponds to a $\text{Sm } 2p \rightarrow 5d$ transition. The intensity of the white line depends on the number of unoccupied states in the d orbitals. In our samples, the most intense white line is associated to the $\text{Sm}(\text{OH})_3$ nanorod sample, which is not affected by OA. In this sample we have Sm^{3+} ions with $4f^5 5d^0 6s^0$ configuration and 5d orbitals fully empty that correspond to the most intense L_3 -edge white line. Adding the OA, some OH^- anions are removed and one electron is left behind when a hydroxyl group is released in $\text{Sm}(\text{OH})_3$ samples. The latter electron will fill 5d orbitals, rather than higher energy 4f orbitals. Moreover, when vacancies increase following the concentration of the surfactant, the occupation of Sm 5d orbitals will also increase. As a consequence the intensity of the white line of $\text{Sm}(\text{OH})_3$ samples has to decrease. When in the modified sample the concentration of Sm ions with one 5d electron is high enough, a ferromagnetic behavior emerges due to the $\text{Sm}(5d^1)\text{-O-Sm}(5d^1)$ superexchange.

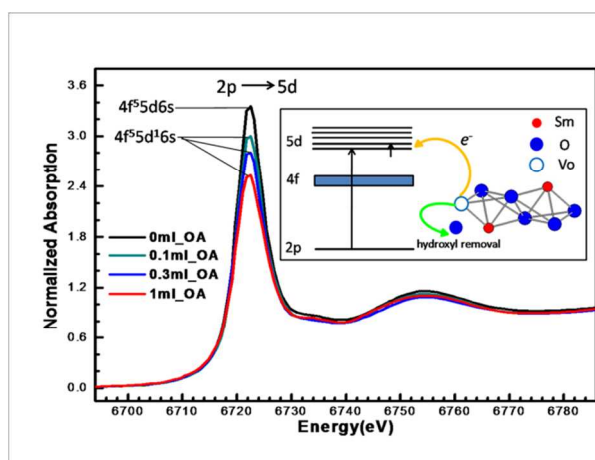


Fig. 5 Sm L_3 edge XANES spectra of samples shown in Fig. 1. The Inset shows the localization of electrons in 5d orbitals, due to the removal of the hydroxyl groups.

4 Conclusions

In summary, $\text{Sm}(\text{OH})_3$ nanocrystals with different morphologies were successfully synthesized by a facile hydrothermal method, assisted with OA surface modification. We show that rod-like $\text{Sm}(\text{OH})_3$ nanocrystals can be tuned to sheet- or disc-like shapes depending on the concentration of oleic acid. Moreover, a magnetic response, i.e., a weak ferromagnetism with a magnetization of about 0.14 and 0.12 emu/g at 300 and 5 K, is measured in $\text{Sm}(\text{OH})_3$ nanodiscs, at variance of the non-magnetism of nanorods and nanosheets. Finally, the XANES analysis points out a correlation between magnetism and morphology of $\text{Sm}(\text{OH})_3$ nanocrystals. The weak magnetic behavior is generated by the surfactant-induced surface modification and the related change of the electron's localization. These results provide useful insights to better understand the magnetism of samarium compounds and open an easy way to synthesize new multifunctional materials for many technological applications.

Acknowledgements

This work was financially supported by the National Basic Research Program of China (2009 CB930804, 2012CB825800 and 2014CB848900), the Science Fund for Creative Research Groups of the NSFC (11321503), the Knowledge Innovation Program of the Chinese Academy of Sciences (KJCX2-YW-N42), the Key Important Project of the National Natural Science Foundation of China (10734070), the National Natural Science Foundation of China (11179023, 11179001 and U1232131) and the Fundamental Research Funds for the Central Universities (WK2310000035). L.S. thanks the recruitment program of global experts and the CAS Hundred Talent Program of China.

Notes and references

- ^aNational Synchrotron Radiation Laboratory, University of Science and Technology of China, Hefei, 230029, China.
- ^bE-mail: chuws@ustc.edu.cn; wuzy@ustc.edu.cn; Fax: +86 5513602017; Tel: +86 5513602017
- ^cBeijing Synchrotron Radiation Facility, Institute of High Energy Physics, Beijing, 100049, China
- ^dHefei National Laboratory for Physical Science at the Microscale, University of Science and Technology of China, Hefei, 230026, China
- ^eIstituto Nazionale di Fisica Nucleare, Laboratori Nazionali di Frascati, P.O. Box 13, 00044, Frascati, Italy
- I. Sevonkaev, V. Privman and D. J. Goia, *Solid State Electrochem.*, 2013, **17**, 279.
- SE. Habas, H. Lee, V. Radmilovic, GA. Somorjai and P. Yang, *Nat. Mater.*, 2007, **6**, 692.
- YW. Jun, JS. Choi and J. Cheon, *Angew. Chem. Int. Ed.*, 2006, **45**, 3414.
- A. Heller, O. Ronitz, A. Barkleit, G. Bernhard and JU. Ackermann, *Appl. Spectrosc.*, 2010, **64**, 8.
- S. Sivakumar, FCJM. van Veggel and PS. May, *J. Am. Chem. Soc.*, 2007, **129**, 620.
- S. Kobayashi, M. Sugiura and H. Kitagawa, *Chem. Rev.*, 2002, **102**, 2227.
- G. Xiao, Z. Jiang, H.Li, C. Xia and L. Chen, *Fuel Cells*, 2009, **09**, 650.
- F. Geng, H. Xin, Y. Matsushita, R. Ma, M. Tanaka, F. Izumi, N. Iyi and T. Sasaki, *Chem. Eur. J.*, 2008, **14**, 9255.
- F. Geng, Y. Matsushita, R. Ma and H. Xin, *J. Am. Chem. Soc.*, 2008, **130**, 16344.
- L. J. McIntyre, J. Laura, L. K. Jackson, and A. M. Fogg, *Journal of Physics and Chemistry of Solids*, 2008, **69**, 1070.
- L. Poudret, T. J. Prior, L. J. McIntyre and A. M. Fogg, *Chemistry of Materials*, 2008, **20**, 7447.
- B. Sels, D. De Vos, M. Buntinx, F. Pierard, A. Kisch-De Mesmaeker and P. Jacobs, *Nature*, 1999, **400**, 855.
- A. Patra, G. A. Baker, and S. N. Baker, *Journal of luminescence*, 2005, **111**, 105.
- P. Ghosh, S. Kundu, A. Kar, K. V. Ramanujachary, S. Lofland and A. Patra, *Journal of Physics D: Applied Physics*, 2010, **43**, 405401.
- J. Yang, C. Li, Z. Quan, C. Zhang, P. Yang, Y. Li and J. Lin, *The Journal of Physical Chemistry C*, 2008, **112**, 12777.
- O. Sartor, P. Hoskin and OS. Bruland, *Cancer Treatment Reviews*, 2013, **39**, 18.
- T. M. Pan, C. C. Huang, *Applied Surface Science*, 2010, **256**, 7186.
- K. Kendall, *Nature*, 2000, **404**, 233.
- K. C. Nicolaou, S. P. Ellery, J. S. Chen, *Angewandte Chemie International Edition*, 2009, **48**, 7140.
- H. F. Brito, O. L. Malta, M. C. F. C. Felinto, E. E. S. Teotonio, J. F. S. Menezes, C. F. B. Silva and C. A. A. Carvalho, *Journal of alloys and compounds*, 2002, **344**, 293.

- ²¹ T. Mokkelbost, I. Kaus, T. Grande and M. A. Einarsrud, *Chemistry of materials*, 2004, **16**, 5489.
- ²² J. Liu, J. Ye, P. Liu, L. Chen and M. Zhang, *Materials Letters*, 2011, **65**, 143.
- ²³ S. Babu, R. Thanneeru, T. Inerbaev, R. Day, A. E. Masunov, A. Schulte and S. Seal, *Nanotechnology*, 2009, **20**, 085713.
- ²⁴ X. Wang, J. Zhuang, Q. Peng and Y. Li, *Nature*, 2005, 437, 121.
- ²⁵ Y. Mao, T. J. Park, F. Zhang, H. Zhou and S. S. Wong, *Small*, 2007, **3**, 1122.
- ²⁶ D. C. Pan, Q. Wang, S. C. Jiang, L. X.L. Ji and J. An, *J. Adv. Mater.*, 2005, **17**, 176.
- ²⁷ K. J. Ziegler, R. C. Doty, K. P. Johnston, and B. A. Korgel, *J. Am. Chem. Soc.*, 2001, **123**, 7797.
- ²⁸ T. Arita, Y. Ueda, K. Minami, T. Naka, and T. Adschiri, *Ind. Eng. Chem. Res.*, 2010, **49**, 1947.
- ²⁹ J. Zhang, H. Kumagai, K. Yamamura, S. Ohara, S. Takami, A. Morikawa and A. Suda, *Nano letters*, 2011, **11**, 361.
- ³⁰ J. Zhang, S. Ohara, M. Umetsu, T. Naka, Y. Hatakeyama and T. Adschiri, *Advanced Materials*, 2007, **19**, 203.
- ³¹ T. D. Nguyen, D. Mrabet and T. D. Do, *The Journal of Physical Chemistry C*, 2008, **112**, 15226.
- ³² F. Esch, S. Fabris, L. Zhou, T. Montini, C. Africh, P. Fornasiero and R. Rosei, *Science*, 2005, **309**, 752.
- ³³ S. Phokha, S. Pinitsoontorn, P. Chirawatkul, Y. Poo-arporn and S. Maensiri, *Nanoscale research letters*, 2012, **7**, 1.
- ³⁴ T. D. Dunbar, W. L. Warren, B. A. Tuttle, *The Journal of Physical Chemistry B*, 2004, **108**, 908.
- ³⁵ A. Abragam, B. Bleaney, *Electron Paramagnetic Resonance of Transition Ions*; Clarendon Press: Oxford, U.K., 1970.
- ³⁶ J. Chen, Y. Hu, X. Zheng, *Colloids and Surfaces A: Physicochemical and Engineering Aspects*, 2008, **313**, 576.
- ³⁷ S. K. Misra, chapter 7, Spin Hamiltonians and Site Symmetries for Transition Ions, Multifrequency Electron Paramagnetic Resonance, *John Wiley & Sons*, 2011.
- ³⁸ J. Zhang, T. Naka, S. Ohara, K. Kaneko, T. Trevethan, A. Shluger and T. Adschiri, *Physical Review B*, 2011, **84**, 045411.
- ³⁹ A. Bianconi, A. Kotani, K. Okada, R. Giorgi, A. Gargano, A. Marcelli and T. Mijahara, *Phys. Rev. B*, 1988, **38**, 3433.
- ⁴⁰ K.B. Garg, R.K. Singhal, U. Chandra, A. Marcelli and A. Bianconi, *Rev. Sol. State Sci.*, 1990, **4**, 119.
- ⁴¹ J. S. Kang, G. Kim, S. C. Wi, S. S. Lee, S. Choi, S. Cho and B. I. Min, *Physical review letters*, 2005, **94**, 147202.
- ⁴² J. Cheng, W. Chu, W. Xu, J. Zhou, L. Zhang and Z. Wu, *Journal of synchrotron radiation*, 2011, **18**, 723.
- ⁴³ C. R. Natoli, D. K. Misemer and S. Doniach, *Phys. Rev. A.*, 1980, **22**, 1104.
- ⁴⁴ X. Han, J. Lee and H. I. Yoo, *Physical Review B*, 2009, **79**, 100403.